Discrete flux and velocity fields of probability and their global maps in reaction systems

Cite as: J. Chem. Phys. **149**, 185101 (2018); https://doi.org/10.1063/1.5050808 Submitted: 02 August 2018 . Accepted: 18 October 2018 . Published Online: 09 November 2018

Anna Terebus, Chun Liu, and Jie Liang







ARTICLES YOU MAY BE INTERESTED IN

Perspective: Computational chemistry software and its advancement as illustrated through three grand challenge cases for molecular science

The Journal of Chemical Physics 149, 180901 (2018); https://doi.org/10.1063/1.5052551

Nanoscale domains in ionic liquids: A statistical mechanics definition for molecular dynamics studies

The Journal of Chemical Physics 149, 184502 (2018); https://doi.org/10.1063/1.5054999

Graph theory for automatic structural recognition in molecular dynamics simulations The Journal of Chemical Physics 149, 184102 (2018); https://doi.org/10.1063/1.5045818

The Journal of Chemical Physics

2018 EDITORS' CHOICE







Discrete flux and velocity fields of probability and their global maps in reaction systems

Anna Terebus, 1 Chun Liu, 2 and Jie Liang 1,a)

¹Department of Bioengineering, University of Illinois at Chicago, Chicago, Illinois 60607, USA ²Department of Applied Mathematics, Illinois Institute of Technology, Chicago, Illinois 60616, USA

(Received 2 August 2018; accepted 18 October 2018; published online 9 November 2018)

Stochasticity plays important roles in reaction systems. Vector fields of probability flux and velocity characterize time-varying and steady-state properties of these systems, including high probability paths, barriers, checkpoints among different stable regions, as well as mechanisms of dynamic switching among them. However, conventional fluxes on continuous space are ill-defined and are problematic when at the boundaries of the state space or when copy numbers are small. By re-defining the derivative and divergence operators based on the discrete nature of reactions, we introduce new formulations of discrete fluxes. Our flux model fully accounts for the discreetness of both the state space and the jump processes of reactions. The reactional discrete flux satisfies the continuity equation and describes the behavior of the system evolving along directions of reactions. The species discrete flux directly describes the dynamic behavior in the state space of the reactants such as the transfer of probability mass. With the relationship between these two fluxes specified, we show how to construct timeevolving and steady-state global flow-maps of probability flux and velocity in the directions of every species at every microstate and how they are related to the outflow and inflow of probability fluxes when tracing out reaction trajectories. We also describe how to impose proper conditions enabling exact quantification of flux and velocity in the boundary regions, without the difficulty of enforcing artificial reflecting conditions. We illustrate the computation of probability flux and velocity using three model systems, namely, the birth-death process, the bistable Schlögl model, and the oscillating Schnakenberg model. Published by AIP Publishing. https://doi.org/10.1063/1.5050808

I. INTRODUCTION

Biochemical reactions in cells are intrinsically stochastic. 1-4 When the concentrations of participating molecules are small or the differences in reaction rates are large, stochastic effects become prominent.^{3,5–7} Many stochastic models have been developed to gain understanding of these reaction systems.^{8–12} These models either generate time-evolving landscapes of probabilities over different microstates^{9–12} or generate trajectories along which the systems travel.^{8,13} Vector fields of probability flux and probability velocity are also of significant interest as they can further characterize timevarying properties of the reaction systems, including that of the non-equilibrium steady states. ^{14–19} For example, determining the probability flux can help to infer the mechanism of dynamic switching among different attractors. 20,21 Quantifying the probability flux can also help to characterize the departure of non-equilibrium reaction systems from detailed balance 16,22,23 and can help to identify barriers and checkpoints between different stable cellular states.²⁴ Computing probability fluxes and velocity fields has found applications in studies of stem cell differentiation, 25 cell cycle, 24 and cancer development.^{26,27}

Several discrete models of probability flux and velocity based on continuous-time Markov jump processes associated with the firing of reactions have also been introduced. 20,29,30,32 However, these models have limitations. The models developed in Refs. 20 and 32 account only for outflow fluxes. While the probability of transition to a subsequent microstate after

Models of probability fluxes and velocities in well-mixed mesoscopic chemical reaction systems have been the focus of many studies. 17,18,20,22-24,28-32 They are often based on the formulation of the Fokker-Planck and the Langevin equations, both involving the assumption of Gaussian noise of two moments. ^{17–19,23,24,33} However, these models are not valid when copy numbers of molecular species are small^{28,34–36} as they do not provide a full account of the stochasticity of the system.^{28,34–38} For example, the Fokker-Planck model fails to capture multistability in gene regulation networks with slow switching between the ON and the OFF states.³⁶ These models are also of inadequate accuracy when systems are far from equilibrium.³⁵ Moreover, solving the systems of partial differential equations resulting from the Fokker-Planck and Langevin equations requires explicit boundary conditions for states where one or more molecular species have zero copies. 18 These boundary conditions are ill-defined in the context of Gaussian noise³⁹ and are difficult to impose using the Fokker-Planck/Langevin formulation, or any other continuous models, as reactions cannot occur on boundary states when one or more reactants are exhausted.

a)Electronic mail: jliang@uic.edu.

a reaction jump is accounted for, the inflow flux describing the probability of transition into the current microstate from a previous state is not explicitly considered. The work in Ref. 40 studies the phosphorylation and dephosphorylation process. It introduces a formulation of discrete flux based on a forward finite difference operator. However, this is only applicable to this special system of simple single-species reactions, where there is no mass exchange between the two different molecular types. The models developed in Refs. 29 and 30 are limited to analysis of single reactional trajectories. In addition, the probability flux is often assumed to be associated with reactions that are reversible. 41 While these models offer an in-the-moment view on how probability mass moves in the system by following trajectories generated from reaction events, they do not offer a global picture of the time-evolving probability flux at a specific time or at fixed locations in the state space. To construct the global flow-map of discrete probability flux and velocity, proper formulations of discrete flux and velocity as well as methods to quantify the discrete forward and backward flux between every two states connected by reactions are required.

In this study, we introduce the appropriate formulations of discrete flux and discrete velocity for arbitrary mesoscopic reaction systems. We redefine the derivative operator and discrete divergence based on the discrete nature of chemical reactions. The discreteness of both the state space and the jump processes of reactions is taken into consideration, with the discrete version of the continuity equation satisfied. Our approach allows the quantification of probability flux and velocity at every microstate, as well as the ability in tracing out the outflow probability fluxes and the inflow fluxes as reactions proceeds. In addition, proper boundary conditions are imposed, so vector fields of flux and velocity can be exactly computed anywhere in the discrete state space, without the difficulty of enforcing artificial reflecting conditions at the boundaries. 42 Our method can be used to exactly quantify transfer of probability mass and to construct the global flow-map of the probability flux in all allowed directions of reactions over the entire state space. Results computed using our model can provide useful characterization of the dynamic behavior of the reaction system, including the high probability paths along which the probability mass of the system evolves, as well as properties of their non-equilibrium steady states.

The accurate construction of the discrete probability flux, velocity, and their global flow-maps requires the accurate calculation of the time-evolving probability landscape of the reaction networks. Here we employ the recently developed ACME (Accurate Chemical Master Equation) method 12,43 to compute the exact time-evolving probability landscapes of networks by solving the underlying discrete Chemical Master Equation (dCME). This eliminates potential problems arising from inadequate sampling, where rare events of low probability are difficult to quantify using techniques such as the stochastic simulation algorithm (SSA).8,13,44

This paper is organized as follows. We first briefly discuss the theoretical framework of reaction networks and discrete chemical master equation. We then introduce the concept of ordering of the microstates of the system, the definitions of discrete derivatives and divergence, as well as flux and velocity on

a discrete state space. We further illustrate how time-evolving probability flux and velocity fields can be computed for three classical systems, namely, the birth-death process, 12,45 the bistable Schlögl model, ^{13,46} and the oscillating Schnakenberg system. 18,47,48

II. MODELS AND METHODS

A. Microstates, probability, reaction, and probability vector

1. Microstate and state space

We consider a well-mixed biochemical system with constant volume and temperature. It has n molecular species X_i , $i = 1, \ldots, n$, which participate in m reactions R_k , k = 1, ..., m. The microstate $\mathbf{x}(t)$ of the system at time t is a column vector of copy numbers of the molecular species: $\mathbf{x}(t) \equiv (x_1(t), x_2(t), \dots, x_n(t))^T \in \mathbb{Z}_+^n$, where all values are non-negative integers. All the microstates that the system can reach form the state space $\Omega = \{\mathbf{x}(t)|t \in (0, \infty)\}$. The size of the state space is denoted as $|\Omega|$.

2. Probability and probability landscapes

The probability of the system to be at a particular microstate **x** at time *t* is denoted as $p(\mathbf{x}, t) \in \mathbb{R}_{[0,1]}$. The probability surface or landscape $\mathbf{p}(t)$ over the state space Ω is denoted as $\mathbf{p}(t) = \{p(\mathbf{x}, t) | \mathbf{x} \in \Omega\}$.

3. Reaction, discrete increment, and reaction direction

A reaction R_k takes the general form of

$$R_k:c_{1_k}X_1+\cdots+c_{n_k}X_n\xrightarrow{r_k}c'_{1_k}X_1+\cdots+c'_{n_k}X_n$$

so that R_k brings the system from a microstate \mathbf{x} to $\mathbf{x} + \mathbf{s}_k$, where the stoichiometry vector

$$\mathbf{s}_k \equiv (s_k^1, \dots, s_k^n) \equiv (c'_{1_k} - c_{1_k}, \dots, c'_{n_k} - c_{n_k})$$

gives the unit vector of the discrete increment of reaction R_k . \mathbf{s}_k also defines the direction of the reaction R_k . In a wellmixed mesoscopic system, the reaction propensity function $A_k(\mathbf{x})$ is determined by the product of the intrinsic reaction rate r_k and the combinations of relevant reactants in the current microstate x,

$$A_k(\mathbf{x}) = r_k \prod_{l=1}^n \binom{x_l}{c_{lk}}.$$

4. Discrete chemical master equation and boundary states

The discrete Chemical Master Equation (dCME) is a set of linear ordinary differential equations describing the changes of probability over time at each microstate of the system.^{8,49–51} The dCME for an arbitrary microstate $\mathbf{x} = \mathbf{x}(t)$ can be written in the general form as

$$\frac{\partial p(\mathbf{x},t)}{\partial t} = \sum_{k=1}^{m} [A_k(\mathbf{x} - \mathbf{s}_k)p(\mathbf{x} - \mathbf{s}_k,t) - A_k(\mathbf{x})p(\mathbf{x},t)],$$
$$\mathbf{x} - \mathbf{s}_k, \mathbf{x} \in \Omega. \tag{1}$$

It is possible that only a subset or none of the permissible reactions can occur at a particular state \mathbf{x} if it is at the boundary of the state space Ω , where the number of reactants is inadequate. Specifically, we define *the boundary states* $\partial \Omega_k$ for reaction k as the states where reaction R_k cannot happen,

$$\partial \Omega_k \equiv \{ \mathbf{x} = (x_1, \dots, x_i, \dots, x_n) | \text{ there exist } i : x_i < c_{i_k} \}.$$
(2

We define the overall boundary states as $\partial \Omega \equiv \bigcup_{k=1}^{m} \partial \Omega_k$.

5. Reactional probability vector and its time-derivative

We can consider each of the k-th reactions separately and decompose the right-hand side of Eq. (1) into m components, one for each reaction, $k = 1 \dots m$,

$$\frac{\partial p_k(\mathbf{x}, t)}{\partial t} = A_k(\mathbf{x} - \mathbf{s}_k)p(\mathbf{x} - \mathbf{s}_k, t) - A_k(\mathbf{x})p(\mathbf{x}, t). \tag{3}$$

 $\partial p(\mathbf{x},t)/\partial t$ in Eq. (1) therefore can also be written as

$$\frac{\partial p(\mathbf{x},t)}{\partial t} = \sum_{k=1}^{m} \frac{\partial p_k(\mathbf{x},t)}{\partial t}.$$

Any of the *m* reactions can alter the value of $p(\mathbf{x}, t)$ as specified by Eq. (3). While the probability $p(\mathbf{x}, t)$ is a scalar, we define the reactional probability vector $\mathbf{p}(\mathbf{x}, t)$ such that

$$\mathbf{p}(\mathbf{x},t) = (p_1(\mathbf{x},t), \dots, p_m(\mathbf{x},t)) \in \mathbb{R}^m, \tag{4}$$

with $p(\mathbf{x}, t) = \mathbf{p}(\mathbf{x}, t) \cdot \mathbf{1} = (p_1(\mathbf{x}, t), \dots, p_m(\mathbf{x}, t)) \cdot (1, \dots, 1)^T$ = $\sum_{k=1}^{m} p_k(\mathbf{x}, t)$. We also define the *time-derivative of the probability vector* $\partial \mathbf{p}(\mathbf{x}, t)/\partial t$ as

$$\frac{\partial \mathbf{p}(\mathbf{x},t)}{\partial t} \equiv \left(\frac{\partial p_1(\mathbf{x},t)}{\partial t}, \dots, \frac{\partial p_m(\mathbf{x},t)}{\partial t}\right),\,$$

and we have

$$\frac{\partial p(\mathbf{x},t)}{\partial t} = \left(\frac{\partial p_1(\mathbf{x},t)}{\partial t}, \dots, \frac{\partial p_m(\mathbf{x},t)}{\partial t}\right) \cdot (1,\dots,1)^T$$
$$= \frac{\partial \mathbf{p}(\mathbf{x},t)}{\partial t} \cdot \mathbf{1} = \sum_{k=1}^m \frac{\partial p_k(\mathbf{x},t)}{\partial t}.$$

B. Ordering microstates, directional derivative, and discrete divergence

1. Ordering microstates

As the microstates are discrete and the stochastic jumps are dictated by the discrete increments $\{s_k\}$ of reactions, we introduce *discrete partial derivative* and *discrete divergence* to describe the effect of specific reactions.

First, we imposed an unambiguous order relationship "<" over all microstates. We impose an ascending order on the microstates $\mathbf{x}^0 < \mathbf{x}^1 < \cdots < \mathbf{x}^{|\Omega|}$ that is maintained at all time such that for each pair of states $\mathbf{x}^i \neq \mathbf{x}^j$, either $\mathbf{x}^i < \mathbf{x}^j$ or $\mathbf{x}^j < \mathbf{x}^i$ holds, but not both. There are many ways to impose such an ordering. Without loss of generality, we can first use the lexicographic order, so the microstates are initially sorted by species alphabetically and then by increasing number of molecules of the species. Other ordering schemes are also possible.

2. Discrete partial derivative

We now consider the reactional component $p_k(\mathbf{x}, t)$ of the probability of the state \mathbf{x} [see Eq. (4)]. For reaction R_k , the only possible change in \mathbf{x} is determined by its discrete increment of \mathbf{s}_k .

We first consider the case when the state $\mathbf{x} - \mathbf{s}_k$ preceding the reaction R_k and the state \mathbf{x} after the reaction have the order $\mathbf{x} - \mathbf{s}_k < \mathbf{x}$. This also implies $\mathbf{x} < \mathbf{x} + \mathbf{s}_k$. In this case, the direction of the reaction coincides with the direction of the imposed ordering of the microstates [Fig. 1(a)]. We define the discrete partial derivative $\Delta p_k(\mathbf{x}, t)/\Delta \mathbf{x}_k$ of $p_k(\mathbf{x}, t)$ over the discrete states in the direction \mathbf{s}_k of reaction R_k as

$$\frac{\Delta p_k(\mathbf{x}, t)}{\Delta \mathbf{x}_k} \equiv p_k(\mathbf{x}, t) - p_k(\mathbf{x} - \mathbf{s}_k, t), \tag{5}$$

if $\mathbf{x} - \mathbf{s}_k < \mathbf{x} < \mathbf{x} + \mathbf{s}_k$.

We now consider the case when $\mathbf{x} < \mathbf{x} - \mathbf{s}_k$, namely, when the state $\mathbf{x} - \mathbf{s}_k$ preceding reaction R_k and the state \mathbf{x} after R_k are ordered such that the after-reaction state \mathbf{x} is placed prior to the before-reaction state $\mathbf{x} - \mathbf{s}_k$. This also implies $\mathbf{x} + \mathbf{s}_k < \mathbf{x}$ [Fig. 1(b)]. In this case, the discrete partial derivative $\Delta p_k(\mathbf{x}, t)/\Delta \mathbf{x}_k$ is defined as

$$\frac{\Delta p_k(\mathbf{x}, t)}{\Delta \mathbf{x}_k} \equiv -(p_k(\mathbf{x}, t) - p_k(\mathbf{x} + \mathbf{s}_k, t)),\tag{6}$$

if $\mathbf{x} + \mathbf{s}_k < \mathbf{x} < \mathbf{x} - \mathbf{s}_k$. The negative sign "–" indicates that the direction of the reaction R_k is opposite to the direction of the imposed order of the states.

3. Discrete divergence

We now introduce the *discrete divergence* $\nabla_d \cdot \mathbf{p}(\mathbf{x}, t) \in \mathbb{R}$ for the probability vector $\mathbf{p}(\mathbf{x}, t)$ over the m discrete increments $\{\mathbf{s}_k\}$ of the reactions. Applying Eqs. (5) and (6) to each reactional component $p_i(\mathbf{x}, t)$ of $\mathbf{p}(\mathbf{x}, t)$ defined in Eq. (4), the discrete divergence $\nabla_d \cdot \mathbf{p}(\mathbf{x}, t)$ at \mathbf{x} is the sum of all discrete partial derivatives along the directions of reactions,

$$\nabla_{d} \cdot \mathbf{p}(\mathbf{x}, t) \equiv \sum_{k=1}^{m} \frac{\Delta p_{k}(\mathbf{x}, t)}{\Delta \mathbf{x}_{k}}.$$
 (7)

Ascending order of the microstates

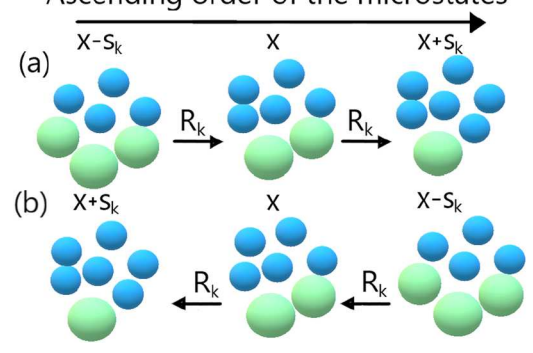


FIG. 1. Ordering of microstates: (a) when the order of the state preceding the reaction R_k and the state after the reaction coincides with the imposed ascending order of microstates, we have $\mathbf{x} - \mathbf{s}_k < \mathbf{x} < \mathbf{x} + \mathbf{s}_k$ and (b) when the order of the state preceding the reaction R_k and the state after the reaction is in the opposite direction to the ascending order of the microstates, we have $\mathbf{x} + \mathbf{s}_k < \mathbf{x} < \mathbf{x} - \mathbf{s}_k$.

C. Discrete flux and velocity at a fixed microstate

1. Single-reactional flux

There are two types of reaction events affecting flux between two states \mathbf{x} and $\mathbf{x} + \mathbf{s}_k$: reactions generating flux flowing from \mathbf{x} to $\mathbf{x} + \mathbf{s}_k$ and reactions generating flux flowing from $\mathbf{x} + \mathbf{s}_k$ to \mathbf{x} . The ordering of the microstates enables unique definition of the type of events that the firing of a reaction R_k belongs to. For any two states \mathbf{x} and $\mathbf{x} + \mathbf{s}_k$, only one of the two orderings is possible: we have either $\mathbf{x} < \mathbf{x} + \mathbf{s}_k$ or $\mathbf{x} + \mathbf{s}_k < \mathbf{x}$. We define the *single-reactional flux of probability* $J_k(\mathbf{x},t) \in \mathbb{R}$ for reaction R_k at microstate $\mathbf{x} \in \Omega$ as

$$J_k(\mathbf{x}, t) \equiv \begin{cases} A_k(\mathbf{x}) p(\mathbf{x}, t) & \mathbf{x} < \mathbf{x} + \mathbf{s}_k, \\ A_k(\mathbf{x} - \mathbf{s}_k) p(\mathbf{x} - \mathbf{s}_k, t) & \mathbf{x} < \mathbf{x} - \mathbf{s}_k. \end{cases}$$
(8)

 $J_k(\mathbf{x}, t)$ depicts the change in $p(\mathbf{x}, t)$ at the state \mathbf{x} due to one firing of reaction R_k . If $\mathbf{x} < \mathbf{x} + \mathbf{s}_k$, $J_k(\mathbf{x}, t)$ depicts the outward flux (outflux) of probability due to one firing of reaction R_k at \mathbf{x} to bring the system from \mathbf{x} to $\mathbf{x} + \mathbf{s}_k$. If $\mathbf{x} < \mathbf{x} - \mathbf{s}_k$, $J_k(\mathbf{x}, t)$ depicts the inward flux (influx) of probability due to one firing of reaction R_k at $\mathbf{x} - \mathbf{s}_k$ to bring the system from $\mathbf{x} - \mathbf{s}_k$ to \mathbf{x} . For any two states connected by a reaction R_k , only one of the two orderings is possible as the imposed ordering of the states

is unique. Therefore, the single-reactional flux can be applied to all microstates in a self-consistent manner. It also accounts for all reactions as $J_k(\mathbf{x},t)$ can be defined for every reaction R_k . The *single-reactional* R_k *velocity* is defined correspondingly as

$$v_k(\mathbf{x}, t) \equiv J_k(\mathbf{x}, t)/p(\mathbf{x}, t).$$

2. Flux at boundary states

No reactions are possible if any of the reactant molecules is unavailable or if its copy number is inadequate. If $\mathbf{x} < \mathbf{x} + \mathbf{s}_k$ [Fig. 1(a)], but $\mathbf{x} \in \partial \Omega_k$ [Eq. (2)], reaction R_k cannot happen, and we have $J_k(\mathbf{x}, t) = 0$. If $\mathbf{x} < \mathbf{x} - \mathbf{s}_k$ [Fig. 1(b)], but $\mathbf{x} - \mathbf{s}_k \in \partial \Omega_k$ [Eq. (2)], reaction R_k cannot happen, and we have $J_k(\mathbf{x}, t) = 0$. We therefore have the following boundary conditions for $J_k(\mathbf{x}, t)$:

$$J_k(\mathbf{x}, t) \equiv \begin{cases} 0 & \mathbf{x} < \mathbf{x} + \mathbf{s}_k \text{ and } \mathbf{x} \in \partial \Omega_k, \\ 0 & \mathbf{x} < \mathbf{x} - \mathbf{s}_k \text{ and } \mathbf{x} - \mathbf{s}_k \in \partial \Omega_k. \end{cases}$$

3. Discrete derivative of J_k

Similar to Eqs. (5) and (6), the directional derivative of single-reactional flux $\Delta J_k(\mathbf{x}, t)/\Delta \mathbf{x}_k$ of $J_k(\mathbf{x}, t)$ along the direction \mathbf{s}_k of reaction R_k is defined as follows:

$$\frac{\Delta J_k(\mathbf{x},t)}{\Delta \mathbf{x}_k} \equiv \begin{cases} A_k(\mathbf{x}) p(\mathbf{x},t) - A_k(\mathbf{x} - \mathbf{s}_k) p(\mathbf{x} - \mathbf{s}_k,t) & \text{if} \quad \mathbf{x} - \mathbf{s}_k < \mathbf{x}, \\ -(A_k(\mathbf{x} - \mathbf{s}_k) p(\mathbf{x} - \mathbf{s}_k,t) - A_k(\mathbf{x} - \mathbf{s}_k + \mathbf{s}_k) p(\mathbf{x} - \mathbf{s}_k + \mathbf{s}_k,t)) & \text{if} \quad \mathbf{x} < \mathbf{x} - \mathbf{s}_k. \end{cases}$$

With simplifications from the trivial identity $-\mathbf{s}_k + \mathbf{s}_k = 0$, the two expressions of $\Delta J_k(\mathbf{x}, t)/\Delta \mathbf{x}_k$ can be combined into one,

$$\frac{\Delta J_k(\mathbf{x}, t)}{\Delta \mathbf{x}_k} \equiv A_k(\mathbf{x}) p(\mathbf{x}, t) - A_k(\mathbf{x} - \mathbf{s}_k) p(\mathbf{x} - \mathbf{s}_k, t)
= -\frac{\partial p_k(\mathbf{x}, t)}{\partial t}.$$
(9)

4. Total reactional flux, divergence, and continuity equation

We now define the *total reactional flux* or r-flux $\mathbf{J}_r(\mathbf{x}, t)$, which describes the probability flux at a microstate \mathbf{x} at time t,

$$\mathbf{J}_r(\mathbf{x},t) \equiv (J_1(\mathbf{x},t), \dots, J_m(\mathbf{x},t)) \in \mathbb{R}^m. \tag{10}$$

Intuitively, the r-flux $\mathbf{J}_r(\mathbf{x}, t)$ is the vector of rate change of the probability mass at \mathbf{x} in directions of all reactions. Similar to Eq. (7), we have the *discrete divergence* of $\mathbf{J}_r(\mathbf{x}, t)$ at the microstate \mathbf{x} ,

$$\nabla_{d} \cdot \mathbf{J}_{r}(\mathbf{x}, t) \equiv \sum_{k=1}^{m} \frac{\Delta J_{k}(\mathbf{x}, t)}{\Delta \mathbf{x}_{k}}.$$
 (11)

From Eq. (9), we have

$$\nabla_d \cdot \mathbf{J}_r(\mathbf{x}, t) = \sum_{k=1}^m [A_k(\mathbf{x})p(\mathbf{x}, t) - A_k(\mathbf{x} - \mathbf{s}_k)p(\mathbf{x} - \mathbf{s}_k, t)].$$
(12)

Similar to its continuous version,^{31,52} the discrete continuity equation for the probability mass insists that

$$\nabla_d \cdot \mathbf{J}_r(\mathbf{x}, t) = -\frac{\partial p(\mathbf{x}, t)}{\partial t}.$$
 (13)

From Eqs. (11), (13), and (1), it is clear that r-flux $\mathbf{J}_r(\mathbf{x}, t)$ satisfies the continuity equation. The probability mass flows simultaneously along all m directions, with the continuity equation satisfied at all time.

5. Single-reactional species flux and stoichiometric projection

The reactional probability flux $J_k(\mathbf{x}, t)$ along the direction of reaction R_k defined in Eq. (8) can be further decomposed into components of individual species. With the predetermined stoichiometry $\mathbf{s}_k = (s_k^1, \dots, s_k^n)$, we define the *stoichiometric projection* of $J_k(\mathbf{x}, t)$ into the component of the j-th species X_j as

$$J_k^j(\mathbf{x},t) \equiv s_k^j J_k(\mathbf{x},t).$$

The set of scalar components of all species $\{J_k^j(\mathbf{x},t)\}$ can be used to form a vector $\mathbf{J}_k(\mathbf{x},t) \in \mathbb{R}^n$, which we call *the single-reaction species flux*,

$$\mathbf{J}_k(\mathbf{x},t) \equiv (J_k^1(\mathbf{x},t),\ldots,J_k^n(\mathbf{x},t)) = \mathbf{s}_k J_k(\mathbf{x},t) \in \mathbb{R}^n.$$

The single-reaction species velocity of probability is defined correspondingly as $\mathbf{v}_k(\mathbf{x}, t) \equiv \mathbf{J}_k(\mathbf{x}, t)/p(\mathbf{x}, t)$.

6. Total species flux and velocity

The *total species flux* or *s-flux* $\mathbf{J}_s(\mathbf{x}, t) \in \mathbb{R}^n$ is the sum of all k single-reaction species flux vectors at a microstate $\mathbf{x} \in \mathbb{R}^n$,

$$\mathbf{J}_{s}(\mathbf{x},t) \equiv \sum_{k=1}^{m} \mathbf{J}_{k}(\mathbf{x},t) = \sum_{k=1}^{m} \mathbf{s}_{k} J_{k}(\mathbf{x},t) \in \mathbb{R}^{n}.$$
 (14)

The total species velocity for probability is defined accordingly as

$$\mathbf{v}_{s}(\mathbf{x},t) = \sum_{k=1}^{m} \mathbf{J}_{s}(\mathbf{x},t)/p(\mathbf{x},t).$$
 (15)

The s-flux $\mathbf{J}_s(\mathbf{x}, t)$ is different from the r-flux $\mathbf{J}_r(\mathbf{x}, t)$ defined in Eq. (12). Reaction-centric $\mathbf{J}_r(\mathbf{x}, t) \in \mathbb{R}^m$ characterizes the total probability flux at the current state in the directions of all reactions, while species-centric $\mathbf{J}_s(\mathbf{x}, t) \in \mathbb{R}^n$ sums up the contributions of every reaction to the probability flux at the state \mathbf{x} in the directions of all species.

D. Flux of reversible reaction

1. Flux of reversible reactions system

We now discuss probability flux in reversible reaction systems that has been previously studied 16,53 and how they are related to fluxes formulated here. For a pair of the reactions, its directionality needs to be specified upfront, namely, which reaction is the forward reaction R^+ and which is the reversed reaction R^- ,

$$R^+: c_1X_1 + \dots + c_nX_n \xrightarrow{r^+} c_1'X_1 + \dots + c_n'X_n,$$

$$R^-: c_1'X_1 + \dots + c_n'X_n \xrightarrow{r^-} c_1X_1 + \dots + c_nX_n.$$

Let $\mathbf{s} = (c_1' - c_1, \ldots, c_n' - c_n)$ be the stoichiometry of reaction R^+ and $-\mathbf{s}$ be the stoichiometry of reaction R^- . The flux J described in Refs. 16 and 53 is the net flux between \mathbf{x} and $\mathbf{x} + \mathbf{s}$. It is specified as the difference between the forward flux at $\mathbf{x} J^+(\mathbf{x}, t) = r^+ \prod_{l=1}^n \binom{x_l}{c_l} p(\mathbf{x}, t)$ generated by the forward reaction

 R^+ and the reverse flux at $\mathbf{x} + \mathbf{s} J^-(\mathbf{x} + \mathbf{s}, t) = r^- \prod_{l=1}^n \binom{x_l + s_l}{c_l'} p(\mathbf{x} + \mathbf{s}, t)$ generated by the reverse reaction R^- , both connecting \mathbf{x} and $\mathbf{x} + \mathbf{s}, t^{16,53}$

$$J(\mathbf{x},t) = r^{+} \prod_{l=1}^{n} {x_{l} \choose c_{l}} p(\mathbf{x},t) - r^{-} \prod_{l=1}^{n} {x_{l} + s_{l} \choose c'_{l}} p(\mathbf{x} + \mathbf{s},t). \quad (16)$$

2. Conversion between single-reactional species flux and flux in a pair of reversible reaction system

The flux $J(\mathbf{x}, t)$ for a pair of reversible reactions above can be related to the s-flux $\mathbf{J}_s(\mathbf{x}, t)$ of Eq. (14) by examining the projection of the $J(\mathbf{x}, t)$ in Eq. (16) to individual species. Specifically, with the stoichiometry \mathbf{s} , the projection

of the flux of Eq. (16) to the component of the *j*-th species X_i is

$$\mathbf{J}(\mathbf{x},t) = \mathbf{s}J(\mathbf{x},t) = \mathbf{s}r^{+} \prod_{l=1}^{n} {x_{l} \choose c_{l}} p(\mathbf{x},t) - \mathbf{s}r^{-}$$

$$\times \prod_{l=1}^{n} {x_{l} + s_{l} \choose c'_{l}} p(\mathbf{x} + \mathbf{s},t) \in \mathbb{R}^{n}. \quad (17)$$

When the direction of the forward reaction R^+ coincides with the ascending order of the states, one firing of R^+ with the stoichiometry vector \mathbf{s} at the state \mathbf{x} brings the system to the state $\mathbf{x} + \mathbf{s}$ in the direction of the ascending order. From Eq. (14), the s-flux $\mathbf{J}_s(\mathbf{x}, t)$ for (R^+, R^-) is $\mathbf{J}_s(\mathbf{x}, t) = \mathbf{s} r^+ \prod_{l=1}^n \binom{x_l}{c_l} p(\mathbf{x}, t) - \mathbf{s} r^- \prod_{l=1}^n \binom{x_l+s_l}{c_l'} p(\mathbf{x} + \mathbf{s}, t)$. In this case, the projection of the reversible reaction flux by Eq. (17) is identical to the s-flux by Eq. (14) at the state \mathbf{x} .

When the direction of the forward reaction R^+ is opposite to the ascending order of the states, one firing of R^- with the stoichiometry vector $-\mathbf{s}$ at the state $\mathbf{x} + \mathbf{s}$ brings the system to the state \mathbf{x} in the direction of the ascending order. From Eq. (14), the s-flux $\mathbf{J}_s(\mathbf{x} + \mathbf{s}, t)$ for (R^+, R^-) is $\mathbf{J}_s(\mathbf{x} + \mathbf{s}, t) = \mathbf{s}r^+ \prod_{l=1}^n \binom{x_l}{c_l} p(\mathbf{x}, t) - \mathbf{s}r^- \prod_{l=1}^n \binom{x_l+s_l}{c_l'} p(\mathbf{x} + \mathbf{s}, t)$. In this case, the projection of the reversible reaction flux by Eq. (17) is identical to s-flux by Eq. (14) at the state $\mathbf{x} + \mathbf{s}$.

III. RESULTS

Below we illustrate how time-evolving and steady-state flux and velocity fields of the probability mass can be computed for three model systems, namely, the birth-death process, the bistable Schlögl model, and the oscillating Schnakenberg system. The underlying discrete Chemical Master Equation (dCME) [Eq. (1)] of these models is solved using the recently developed ACME method. 12,43 The resulting exact probability landscapes of these models are used to compute the flux and the velocity fields.

A. The birth and death process

The birth-death process is a simple but ubiquitous process of the synthesis and degradation of molecule of a single specie. 12,45 The reaction schemes and rate constants examined in this study are specified as follows:

$$R_1: \emptyset \xrightarrow{r_1} X, \quad r_1 = 1,$$

 $R_2: X \xrightarrow{r_2} \emptyset, \quad r_2 = 0.025.$

Below we use k as the index of the two reactions.

1. Ordering microstates

The microstate in this system is defined by the copy number x of the molecular specie X. We order the microstates in the direction of increasing copy numbers of x, namely, $(x = 0) < (x = 1) < (x = 2) \cdot \cdot \cdot$.

2. Discrete increment and reaction direction

Reaction R_1 brings the system from the state x to the state x + 1, in the direction of increasing order of the microstates.

Its discrete increment is $s_1 = 1$. Reaction R_2 brings the system from the state x to the state x - 1, in the direction of decreasing order of the microstates. Its discrete increment is therefore $s_2 = -1$.

3. Discrete chemical master equation

Following Eq. (1), the discrete chemical master equation for this system can be written as

$$\partial p(x,t)/\partial t = r_1 p(x,t) - r_1 p(x-1,t) - r_2 (x+1)$$

 $\times p(x+1,t) + r_2 x p(x,t).$ (18)

4. Single-reactional flux, velocity, and boundary conditions

The single-reactional flux $J_k(x, t) \in \mathbb{R}$ can be written as

$$J_1(x,t) = r_1 p(x,t), \ J_2(x,t) = r_2(x+1)p(x+1,t).$$
 (19)

Here $x = 0, 1, \dots$ No special boundary conditions are required for this system as $J_1(x, t)$ and $J_2(x, t)$ at the boundary x = 0 take the values specified by Eq. (19). The single-reactional velocity $v_k(x,t) \in \mathbb{R}$ can be written as $v_1(x,t) = J_1(x,t)/p(x,t)$ and $v_2(x, t) = J_2(x, t)/p(x, t).$

5. Discrete partial derivative

The imposed ordering of the microstates implies $x < x + s_1$ as $s_1 = 1$ and x < x + 1. By Eq. (5), the derivative $\Delta J_1(x, t)/\Delta x_1$ of the single-reactional flux function J_1 is

$$\frac{\Delta J_1(x,t)}{\Delta x_1} = J_1(x,t) - J_1(x - s_1,t)$$
$$= r_1 p(x,t) - r_1 p(x - 1,t)$$

The imposed ordering of the microstates also has $x < x - s_2$ as $s_2 = -1$ and x < x + 1. By Eq. (6), the derivative $\Delta J_2(x, t)/\Delta x_2$ of the single-reactional flux function J_2 is

$$\begin{split} \frac{\Delta J_2(x,t)}{\Delta x_2} &= -(J_2(x,t) - J_2(x+s_2,t)) \\ &= -(r_2(x+1)p(x+1,t) - r_2(x)p(x,t)). \end{split}$$

6. Total reactional flux, discrete divergence, and continuity equation

Following Eq. (10), the total reactional flux $\mathbf{J}_r(x,t) \in \mathbb{R}^2$ is

$$\mathbf{J}_r(x,t) = (J_1(x,t), J_2(x,t))$$

= $(r_1p(x,t), r_2(x+1)p(x+1,t)).$

The total reactional velocity $\mathbf{v}_r(x,t) \in \mathbb{R}^2$ is $\mathbf{v}_r(x,t)$ $= \mathbf{J}_r(x, t)/p(x, t).$

Following Eq. (7), the discrete divergence $\nabla_d \cdot \mathbf{J}_r(x, t)$ of $\mathbf{J}_r(x,t) \in \mathbb{R}^2$ over the discrete increments s_1 and s_2 can be

$$\nabla_{d} \cdot \mathbf{J}_{r}(x,t) = \sum_{k=1}^{2} \frac{\Delta J_{k}(x,t)}{\Delta x_{k}}$$

$$= r_{1}p(x,t) - r_{1}p(x-1,t)$$

$$- r_{2}(x+1)p(x+1,t) + r_{2}(x)p(x,t). \quad (20)$$

Here the r-flux $J_r(x,t)$ indeed satisfies the continuity equation as we have $\nabla_d \cdot \mathbf{J}_r(x, t) = -\partial p(x, t)/\partial t$ from Eqs. (13), (18),

7. Stoichiometry projection and single-reactional species flux

Since there is only one specie in this system, the stoichiometry projection of $J_k(x, t)$ to the specie X is equal to the single-reactional species flux $\mathbf{J}_k(x,t) \in \mathbb{R}$, which can be written as

$$\mathbf{J}_1(x,t) = r_1 p(x,t)$$
 and $\mathbf{J}_2(x,t) = -r_2(x+1)p(x+1,t)$.

The single-reactional species velocity $\mathbf{v}_k(x,t) \in \mathbb{R}$ can be written as follows: $\mathbf{v}_1(x, t) = J_1(x, t)/p(x, t)$ and $\mathbf{v}_2(x, t)$ $= J_2(x, t)/p(x, t).$

8. Total species flux and velocity

Following Eqs. (14) and (15), the s-flux $J_s(x, t)$ and the total velocity $v_s(x, t)$ are

$$J_s(x,t) = r_1 p(x,t) - r_2(x+1)p(x+1,t),$$

$$v_s(x,t) = J_s(x,t)/p(x,t).$$

When $J_s(x, t) > 0$ and $v_s(x, t) > 0$, the probability mass moves in the direction of increasing copy number of X. This is the direction of the ascending order of microstates we imposed. When $J_s(x, t) < 0$ and $v_s(x, t) < 0$, the probability mass moves in the direction of the decreasing copy number of X. We will further use just simple flux instead of s-flux.

9. Overall behavior of the birth and death system

We examine the behavior of the birth and death process under the initial conditions $p(x = 0)|_{t=0} = 1$ [Fig. 2(a), backside] and that of the uniform distribution [Fig. 2(d), backside].

For the initial condition of $p(x = 0)|_{t=0} = 1$, the probability landscape changes from that with a peak at x = 0 to that with a peak at x = 40 [Fig. 2(a)]. Figure 2(b) shows the heatmap of the flux $J_s(x, t)$, and Fig. 2(c) shows the heatmap of the velocity $v_s(x, t)$. Yellow and red areas represent locations where the probability moves in the positive direction, while white areas represent locations where the flux and velocity both are close to be zero. The flux and velocity of probability mass [Figs. 2(b) and 2(c)] are positive at all time, indicating that the probability mass is moving only in the direction of increasing copy number of x. Moreover, when the probability is non-zero, the probability velocity remains constant at any fixed time t across different microstates. The blue line in Figs. 2(b) and 2(c) corresponds to the peak of the system that changes its location from x = 0 to x = 40.

For the initial condition of the uniform distribution, the probability landscape changes from the constant line to that with a peak at x = 40 [Fig. 2(d)]. Figure 2(e) shows the heatmap of the flux $J_s(x, t)$, and Fig. 2(f) shows the heatmap of the velocity $v_s(x, t)$. Blue areas represent locations where the probability mass moves in the negative direction, yellow and red areas represent locations where the probability moves in the positive direction, while white areas represent locations where

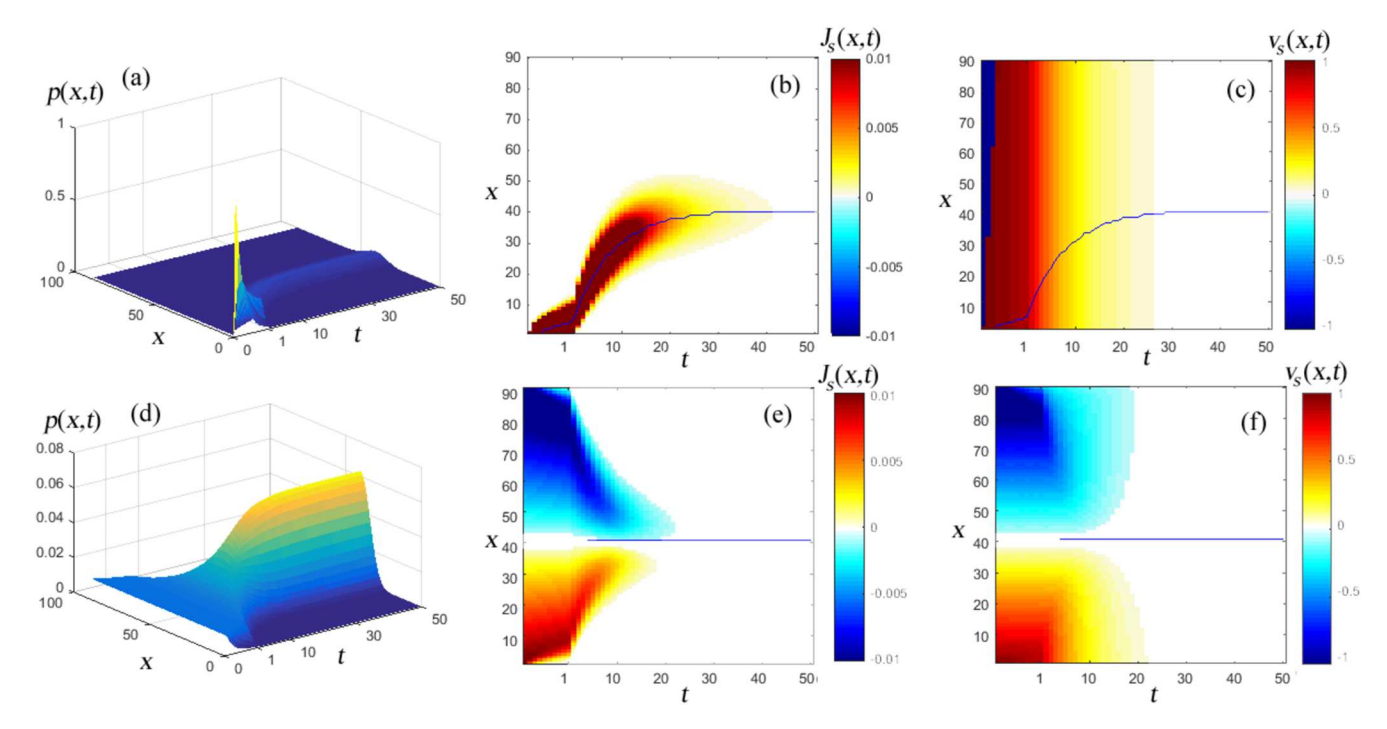


FIG. 2. The time-evolving probability landscape, flux, and velocity of the probability mass of the birth and death system starting from the initial conditions of $p(x = 0)|_{t=0} = 1$ [(a)–(c)] and from the initial conditions of the uniform distribution [(d)–(f)]. (a) and (d): the probability landscape in p(x, t); (b) and (e): the corresponding value of flux $J_s(x, t)$; (c) and (f): the value of velocity $v_s(x, t)$.

the flux and velocity both are equal to zero. Specifically, when x < 40, we have $J_s(x, t) > 0$ and $v_s(x, t) > 0$, namely, the probability mass moves in the direction of increasing copy number of x. By contrast, when x > 40, we have $J_s(x, t) < 0$ and $v_s(x, t) < 0$, indicating that the probability mass moves in the direction of decreasing copy number of x. When x = 40, we have $J_s(x, t) = 0$ and $v_s(x, t) = 0$. Furthermore, the probability velocity at a specific time t is different for different microstates, with the highest velocities located at the boundary of x = 0. The blue line in Figs. 2(e) and 2(f) x = 40 corresponds to the peak of the system, which appears starting at about t = 5.

To solve this problem using the ACME method, we introduced the buffer of capacity x = 92. At the state x = 92 when the buffer is exhausted, no synthesis reaction can occur. Therefore, the flux at the boundary x = 92 is set to zero.

Our birth and death system eventually reaches to a steady state. As expected, the same steady state probability distribution is reached from both initial conditions [shown in different scales in Figs. 2(a) and 2(d)]. At the steady state, the probability landscape has a peak at x = 40. Both the velocity $v_s(x, t)$ and the flux $J_s(x, t)$ converge to zero at the steady state.

B. Bistable Schlögl model

The Schlögl model is a one-dimensional bistable system consisting of an auto-catalytic network involving one molecular specie X and four reactions. He is a canonical model for studying bistability and state-switching. The reaction schemes and kinetic constants examined in this study are specified as follows:

$$R_{1}: A + 2X \xrightarrow{k_{1}} 3X, \quad k_{1} = 6;$$

$$R_{2}: 3X \xrightarrow{k_{2}} A + 2X, \quad k_{2} = 3.6;$$

$$R_{3}: B \xrightarrow{k_{3}} X, \quad k_{3} = 0.25;$$

$$R_{4}: X \xrightarrow{k_{4}} B, \quad k_{4} = 2.95.$$
(21)

Here A and B have constant concentrations a and b, which are set to a = 1 and b = 2, respectively. We set the volume of the system to V = 25.⁴⁶ The rate of reactions are specified as $r_1 = k_1/V$, $r_2 = k_2/V^2$, $r_3 = k_3V$, and $r_4 = k_4$.

1. Ordering microstates

We define the microstates of this system using the copy number x of the molecular specie X. We order the microstates in the direction of increasing copy numbers of X, namely, $(x = 0) < (x = 1) < (x = 2) \cdot \cdot \cdot$.

2. Discrete increment and reaction direction

Reactions R_1 and R_3 bring the system from the state x to the state x + 1, in the direction of increasing order of the microstates. Their discrete increments s_1 and s_3 are $s_1 = 1$ and $s_3 = 1$. Reactions R_2 and R_4 bring the system from the state \mathbf{x} to the state x - 1, in the direction of decreasing order of the microstates. Their discrete increments s_2 and s_4 are therefore $s_2 = -1$ and $s_4 = -1$.

3. Discrete chemical master equation

Following Eq. (1), the discrete chemical master equation for this system can be written as

$$\frac{\partial p(x,t)}{\partial t} = r_1 a \frac{(x-1)(x-2)}{2} p(x-1,t) + r_2 \frac{(x+1)x(x-1)}{6} p(x+1,t) + r_3 b p(x-1,t) + r_4 (x+1) p(x+1,t)
- r_1 a \frac{x(x-1)}{2} p(x,t) - r_2 \frac{x(x-1)(x-2)}{6} p(x,t) - r_3 b p(x,t) - r_4 x p(x,t).$$
(22)

We compute the probability landscape p(x, t) underlying Eq. (22) using the ACME method. ^{12,43}

4. Single-reactional flux, velocity, and boundary conditions

Following Eq. (8), the single-reactional flux $J_k(x, t) \in \mathbb{R}$ can be written as

$$J_1(x,t) = r_1 a \frac{x(x-1)}{2} p(x,t),$$

$$J_2(x,t) = r_2 \frac{(x+1)x(x-1)}{6} p(x+1,t),$$

$$J_3(x,t) = r_3 b p(x,t),$$

$$J_4(x,t) = r_4(x+1) p(x+1,t).$$

We have the single-reactional fluxes $J_1(x, t) = 0$ and $J_2(x, t) = 0$ on the boundary with either x = 0 or x = 1, where reactions R_1 and R_2 cannot happen. The single-reactional fluxes $J_3(x, t)$ and $J_4(x, t)$ are as given above and do not vanish at the boundaries.

The single-reactional velocity $v_k \in \mathbb{R}$ can be written as $v_k(x, t) = J_k(x, t)/p(x, t)$, with k = 1, ..., 4.

5. Discrete partial derivative

The imposed ordering of the microstates has x < x + 1, and therefore, $x < x + s_1$, $x < x - s_2$, $x < x + s_3$, and $x < x - s_4$ as $s_1 = 1$, $s_2 = -1$, $s_3 = 1$, and $s_4 = -1$. According to Eqs. (5) and (6), the derivatives $\Delta J_k(x, t)/\Delta x_k$ of the single-reactional fluxes $\{J_k\}$ are

$$\begin{split} \frac{\Delta J_1(x,t)}{\Delta x_1} &= J_1(x,t) - J_1(x-s_1,t) \\ &= r_1 a \frac{x(x-1)}{2} p(x,t) - r_1 a \frac{(x-1)(x-2)}{2} p(x-1,t), \\ \frac{\Delta J_2(x,t)}{\Delta x_2} &= -(J_2(x,t) - J_2(x+s_2,t)) \\ &= -(r_2 \frac{(x+1)x(x-1)}{6} p(x+1,t) \\ &- r_2 \frac{(x+2)(x+1)x}{6} p(x,t)), \\ \frac{\Delta J_3(x,t)}{\Delta x_3} &= J_3(x,t) - J_3(x-s_3,t) \\ &= -(r_3 b p(x,t) - r_3 b p(x-1,t)), \\ \frac{\Delta J_4(x,t)}{\Delta x_4} &= -(J_4(x,t) - J_4(x+s_4,t)) \\ &= -(r_4(x+1) p(x+1,t) - r_4 x p(x,t)). \end{split}$$

6. Total reactional flux and velocity, discrete divergence, and continuity equation

Following Eq. (10), the total reactional flux $\mathbf{J}_r(x,t) \in \mathbb{R}^4$ is

$$\mathbf{J}_{r}(x,t) = (J_{1}(x,t), J_{2}(x,t), J_{3}(x,t), J_{4}(x,t))$$

$$= (r_{1}a\frac{x(x-1)}{2}p(x,t), r_{2}\frac{(x+1)x(x-1)}{6}$$

$$\times p(x+1,t), r_{3}bp(x,t), r_{4}(x+1)p(x+1,t)).$$

The total reactional velocity $\mathbf{v}_r(x,t) \in \mathbb{R}^4$ is $\mathbf{v}_r(x,t) = \mathbf{J}_r(x,t)/p(x,t)$.

The discrete divergence $\nabla_d \cdot \mathbf{J}_r(x, t)$ of $\mathbf{J}_r(x, t) \in \mathbb{R}^4$ over the discrete increments s_1, s_2, s_3 , and s_4 can be written as

$$\nabla_{d} \cdot \mathbf{J}_{r}(x,t) = \sum_{k=1}^{4} \frac{\Delta J_{k}(x,t)}{\Delta x_{k}} = -\frac{(x-1)(x-2)}{2} r_{1} a p(x-1,t) + r_{1} a \frac{x(x-1)}{2} p(x,t) - r_{2} \frac{(x+1)x(x-1)}{6} p(x+1,t) + r_{2} \frac{x(x-1)(x-2)}{6} p(x,t) - r_{3} b p(x-1,t) + r_{3} b p(x,t) - r_{4}(x+1) p(x+1,t) + r_{4} x p(x,t).$$
(23)

The flux $\mathbf{J}_r(x, t)$ indeed satisfies the continuity equation as we have $\nabla_d \cdot \mathbf{J}_r(x, t) = -\partial p(x, t)/\partial t$ from Eqs. (13), (22), and (23).

7. Stoichiometry projection and single-reactional species flux

Since there is only one specie x in this system, the stoichiometry projection of single-reactional flux $J_k(x, t)$ to x is equal to the single-reactional species flux $J_k(x, t) \in \mathbb{R}$, which

can be written as

$$\mathbf{J}_{1}(x,t) = r_{1}a\frac{x(x-1)}{2}p(x,t),$$

$$\mathbf{J}_{2}(x,t) = -r_{2}\frac{(x+1)x(x-1)}{6}p(x+1,t),$$

$$\mathbf{J}_{3}(x,t) = r_{3}bp(x,t),$$

$$\mathbf{J}_{4}(x,t) = -r_{4}(x+1)p(x+1,t).$$

The single-reactional species velocities $\mathbf{v}_k \in \mathbb{R}$ is $\mathbf{v}_k(x, t) = \mathbf{J}_k(x, t)/p(x, t)$, with k = 1, ..., 4.

8. Total species flux and velocity

Following Eqs. (14) and (15), the total species flux $\mathbf{J}_s(x, t)$ and velocity $\mathbf{v}_s(x, t)$ for the four reactions are

$$J_s(x,t) = r_1 a \frac{x(x-1)}{2} p(x,t) - r_2 \frac{(x+1)x(x-1)}{6}$$
$$\times p(x+1,t) + r_3 b p(x,t) - r_4 (x+1) p(x+1,t),$$

and $v_s(x, t) = J_s(x, t)/p(x, t)$.

9. Overall behavior of the Schlögl system

For the set of parameter values used in Eq. (21), the Schlögl model is bistable. It has two peaks at x = 4 and x = 92. In order to study how switching between the two peaks occur, we examine the behavior of the model under the initial conditions of $p(x = 4)|_{t=0} = 1$ [Fig. 3(a)] and the initial condition of $p(x = 92)|_{t=0} = 1$ [Fig. 3(d)].

For the initial distribution of $p(x = 4)|_{t=0} = 1$, the probability landscape changes from that with a single peak at x = 4 to that with two maximum peaks at x = 4 and x = 92 [Fig. 3(a)]. Figure 3(b) shows the heatmap of the flux $J_s(x, t)$, and Fig. 3(c) shows the heatmap of the velocity $v_s(x, t)$. Yellow and red areas represent locations where the probability moves in the positive direction, while white areas represent locations where the flux and velocity both are close to be zero. The lower blue lines in Figs. 3(b) and 3(c) correspond to the peak at x = 4. They are straight lines as the location of the peak does not

change over time. Another blue line starts to appear at x = 92 at about t = 3 and corresponds to the second peak. At the same time, at around t = 3, we observe the appearance of a minimum of the probability landscape (red line), separating the two maximum peaks. We have $J_s(x, t) > 0$ and $v_s(x, t) > 0$, indicating that the probability moves in the direction of increasing copy number of molecules [Figs. 3(b) and 3(c)] in the majority of the states. In the white region, we have $J_s(x, t) = 0$ and $v_s(x, t) = 0$.

For the first initial condition of $p(x = 92)|_{t=0} = 1$, the probability landscape changes from that with a single peak at x = 92 to that of two peaks at x = 92 and x = 4 [Fig. 3(d)]. Figure 3(e) shows the heatmap of the flux $J_s(x, t)$, and Fig. 3(f) shows the heatmap of the velocity $v_s(x, t)$. Blue areas represent locations where the probability mass moves in the negative direction, while white areas represent locations where the flux and velocity both are equal to zero. The top blue lines in Figs. 3(e) and 3(f) correspond to the peak at x = 92. These are straight lines as the location of this peak does not change over time. Another blue line starts to appear at x = 4 at around t = 3 and corresponds to the second peak. At around t = 3, we also observe the appearance of a minimum on the probability landscape (red line) separating the two maximum peaks. In the blue region, we have $J_s(x, t) < 0$ and $v_s(x, t) < 0$, and the probability moves in the direction of increasing copy number of molecules [Figs. 3(e) and 3(f)] in the majority of states. In the white region, we have $J_s(x, t) = 0$ and $v_s(x, t) = 0$.

In both cases (Fig. 3), the second peak appears after about t = 3. We also observe that the absolute values of the flux driving the system from the system with one peak at x = 4 to the emergence of the second peak at x = 92 and from the system with one peak at x = 92 to the emergence of the second peak at x = 4 are of the same scale.

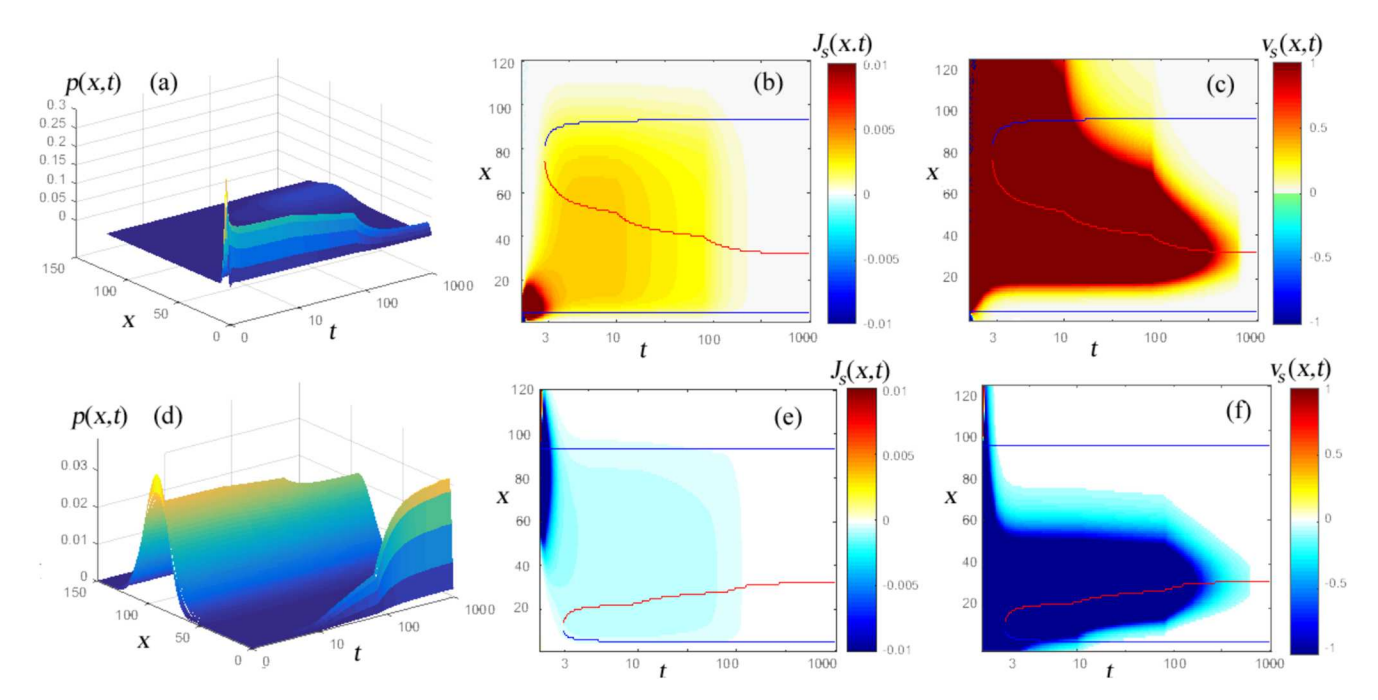


FIG. 3. The time-evolving probability landscape, flux, and velocity of the probability mass in the Schlögl system starting from the initial conditions of $p(x = 4)|_{t=0} = 1$ [(a)–(c)] and from the initial conditions of $p(x = 92)|_{t=0} = 1$ [(d)–(f)]. (a) and (d): the probability landscape in p(x, t); (b) and (e): the corresponding value of flux in $J_s(x, t)$; and (c) and (f): the value of velocity $v_s(x, t)$.

The Schlögl process eventually reaches a steady state. As expected, the same steady state probability distribution is reached from both initial conditions. At the steady state, the probability landscape has two peaks at x = 4 and x = 92. Both the velocity $v_s(x, t)$ and the flux $J_s(x, t)$ converge to zero at the steady state.

C. Schnakenberg model

The Schnakenberg model is a simple chemical reaction system originally constructed to study the behavior of limit cycle.⁵⁵ It provides an important model for analyzing oscillating behavior in reaction systems.^{18,47,48} The reaction scheme and rate constants examined in this study are specified as follows:

$$R_{1}: A \xrightarrow{k_{1}} X_{1}, \quad k_{1} = 1;$$

$$R_{2}: X_{1} \xrightarrow{k_{2}} \emptyset, \quad k_{2} = 1;$$

$$R_{3}: B \xrightarrow{k_{3}} X_{2}, \quad k_{3} = 1;$$

$$R_{4}: X_{2} \xrightarrow{k_{4}} \emptyset, \quad k_{4} = 10^{-2};$$

$$R_{5}: 2X_{1} + X_{2} \xrightarrow{k_{5}} 3X_{1}, \quad k_{5} = 1;$$

$$R_{6}: 3X_{1} \xrightarrow{k_{6}} 2X_{1} + X_{2}, \quad k_{6} = 10^{-2}.$$

Here X_1 and X_2 are molecular species whose copy numbers x_1 and x_2 oscillate, and A and B are reactants with fixed copy numbers. The volume of the system V is set to $V = 10^{-2.55}$ The rate of reactions are specified as $r_1 = k_1$, $r_2 = k_2$, $r_3 = k_3$, $r_4 = k_4$, $r_5 = k_5/V^2$, and $r_6 = k_6/V^2$.

1. Ordering microstates

The microstate $\mathbf{x} = (x_1, x_2)$ in this system is defined by the ordered pair of copy numbers x_1 and x_2 of the molecular species X_1 and X_2 . We impose the ascending order of the microstates first in the direction of the increasing copies of X_1 . At a fixed value of X_1 , we then sort the states in the order of increasing copy number of X_2 . We therefore have $(x_1 = 0, x_2 = 0) < (x_1 = 0, x_2 = 1) < (x_1 = 0, x_2 = 2) < \cdots < (x_1 = 1, x_2 = 0) < (x_1 = 1, x_2 = 1) \cdots$.

2. Discrete increment and reaction direction

The discrete increments s_1 , s_3 , and s_5 of reactions R_1 , R_3 , and R_5 that bring the system in the direction of increasing order of the microstates and the discrete increments s_2 , s_4 , and s_6 of reactions s_2 , s_4 , and s_6 of reactions s_2 , s_4 , and s_6 that bring the system in the direction of the decreasing order of the microstates are listed in Table I.

3. Discrete chemical master equation

Following Eq. (1), the discrete chemical master equation for the system can be written as

$$\frac{\partial p(\mathbf{x},t)}{\partial t} = -r_1 a p(x_1, x_2, t) + r_1 a p(x_1 - 1, x_2, t)
- r_2 x_1 p(x_1, x_2, t) + r_2 (x_1 + 1) p(x_1 + 1, x_2, t)
- r_3 b p(x_1, x_2, t) + r_3 b p(x_1, x_2 - 1, t)
+ r_4 (x_2 + 1) p(x_1, x_2 + 1, t) - r_4 x_2 p(x_1, x_2, t)
+ r_5 \frac{(x_1 - 1)(x_1 - 2)x_2}{2} p(x_1 - 1, x_2 + 1, t)
- r_5 \frac{x_1 (x_1 - 1)x_2}{2} p(x_1, x_2, t)
+ r_6 \frac{(x_1 - 1)x_1 (x_1 + 1)}{6} p(x_1 + 1, x_2 - 1, t)
- r_6 \frac{x_1 (x_1 - 1)(x_1 - 2)}{6} p(x_1, x_2, t).$$
(24)

We compute the probability landscape $p(\mathbf{x}, t)$ underlying Eq. (22) using the ACME method. 12,43

4. Single-reactional flux, velocity, and boundary conditions

The single-reactional flux $J_k(\mathbf{x}, t) \in \mathbb{R}$ can be written as

$$J_{1}(\mathbf{x},t) = r_{1}ap(x_{1},x_{2},t),$$

$$J_{2}(\mathbf{x},t) = r_{2}(x_{1}+1)p(x_{1}+1,x_{2},t),$$

$$J_{3}(\mathbf{x},t) = r_{3}bp(x_{1},x_{2},t),$$

$$J_{4}(\mathbf{x},t) = r_{4}(x_{2}+1)p(x_{1},x_{2}+1,t),$$

$$J_{5}(\mathbf{x},t) = r_{5}\frac{x_{1}(x_{1}-1)x_{2}}{2}p(x_{1},x_{2},t),$$

$$J_{6}(\mathbf{x},t) = r_{6}\frac{(x_{1}-1)x_{1}(x_{1}+1)}{6}p(x_{1}+1,x_{2}-1,t).$$
(25)

We have the single-reactional fluxes $J_5(\mathbf{x}, t) = 0$ and $J_6(\mathbf{x}, t) = 0$ on the boundary with either $\mathbf{x} = (0, 0)$ or $\mathbf{x} = (1, 0)$, where reactions R_5 and R_6 cannot happen. The other single-reactional fluxes are as given above and do not vanish at the boundaries.

The single-reactional velocity $v_k(\mathbf{x}, t) \in \mathbb{R}$ can be written as $v_k(\mathbf{x}, t) = J_k(\mathbf{x}, t)/p(\mathbf{x}, t)$.

5. Discrete partial derivative

The imposed ordering of the microstates has $\mathbf{x} < \mathbf{x} + \mathbf{s}_1$, $\mathbf{x} < \mathbf{x} - \mathbf{s}_2$, $\mathbf{x} < \mathbf{x} + \mathbf{s}_3$, $\mathbf{x} < \mathbf{x} - \mathbf{s}_4$, $\mathbf{x} < \mathbf{x} + \mathbf{s}_5$, and $\mathbf{x} < \mathbf{x} - \mathbf{s}_6$. According to Eqs. (5) and (6), the derivatives $\Delta J_k(\mathbf{x}, t)/\Delta \mathbf{x}_k$ of the single-reactional fluxes J_k can be written as

TABLE I. Schnakenberg system reaction stoichiometry.

Reactions	R_1	R_3	R ₅	R_2	R_4	<i>R</i> ₆
Discrete increments	$\mathbf{s}_1 = (1, 0)$	$\mathbf{s}_3 = (0, 1)$	$\mathbf{s}_5 = (1, -1)$	$\mathbf{s}_2 = (-1, 0)$	$\mathbf{s}_4 = (0, -1)$	$\mathbf{s}_6 = (-1, 1)$

$$\frac{\Delta J_1(\mathbf{x},t)}{\Delta \mathbf{x}_1} = J_1(\mathbf{x},t) - J_1(\mathbf{x} - \mathbf{s}_1,t)
= r_1 a p(x_1, x_2, t) - r_1 a p(x_1 - 1, x_2, t),
\frac{\Delta J_2(\mathbf{x},t)}{\Delta \mathbf{x}_2} = -(J_2(\mathbf{x},t) - J_2(\mathbf{x} + \mathbf{s}_2,t))
= -(r_2(x_1 + 1) p(x_1 + 1, x_2, t) - r_2 x_1 p(x_1, x_2, t)),
\frac{\Delta J_3(\mathbf{x},t)}{\Delta \mathbf{x}_3} = J_3(\mathbf{x},t) - J_3(\mathbf{x} - \mathbf{s}_3,t)
= r_3 b p(x_1, x_2, t) - r_3 b p(x_1, x_2 - 1, t)),
\frac{\Delta J_4(\mathbf{x},t)}{\Delta \mathbf{x}_4} = -(J_4(\mathbf{x},t) - J_4(\mathbf{x} + \mathbf{s}_4,t))
= -(r_4(x_2 + 1) p(x_1, x_2 + 1, t) - r_4 x_2 p(x_1, x_2, t)),
\frac{\Delta J_5(\mathbf{x},t)}{\Delta \mathbf{x}_5} = J_5(\mathbf{x},t) - J_5(\mathbf{x} - \mathbf{s}_5,t)
= r_5 \frac{x_1(x_1 - 1)x_2}{2} p(x_1, (x_2 + 1),t)
- r_5 \frac{(x_1 - 1)(x_1 - 2)x_2}{2} p(x_1 - 1, x_2 + 1, t),
\frac{\Delta J_6(\mathbf{x},t)}{\Delta \mathbf{x}_6} = -(J_6(\mathbf{x},t) - J_6(\mathbf{x} + \mathbf{s}_6,t))
= -(r_6 \frac{(x_1 - 1)x_1(x_1 + 1)}{6} p(x_1 + 1, x_2 - 1, t)
- r_6 \frac{x_1(x_1 - 1)(x_1 - 2)}{6} p(x_1, x_2, t)).$$

6. Total reactional flux and velocity, discrete divergence, and continuity equation

Following Eq. (10), the total reactional flux $\mathbf{J}_r(\mathbf{x},t) \in \mathbb{R}^6$ is

$$\mathbf{J}_r(\mathbf{x},t) = (J_1(\mathbf{x},t), J_2(\mathbf{x},t), J_3(\mathbf{x},t), J_4(\mathbf{x},t), J_5(\mathbf{x},t), J_6(\mathbf{x},t)),$$

where $\{J_k(\mathbf{x}, t)\}$ are as specified in Eq. (25). The total reactional velocity $\mathbf{v}_r(\mathbf{x}, t) \in \mathbb{R}^6$ is $\mathbf{v}_r(\mathbf{x}, t) = \mathbf{J}_r(\mathbf{x}, t)/p(\mathbf{x}, t)$.

The discrete divergence $\nabla_d \cdot \mathbf{J}_r(\mathbf{x}, t)$ of the r-flux $\mathbf{J}_r(\mathbf{x}, t)$ $\in \mathbb{R}^6$ over the discrete increments \mathbf{s}_k can be written as

$$\nabla_d \cdot \mathbf{J}_r(\mathbf{x}, t) = \sum_{k=1}^6 \frac{\Delta J_k(\mathbf{x}, t)}{\Delta \mathbf{x}_k}.$$
 (26)

The r-flux $\mathbf{J}_r(\mathbf{x}, t)$ indeed satisfies the continuity equation as we have $\nabla_d \cdot \mathbf{J}_r(\mathbf{x}, t) = -\partial p(\mathbf{x}, t)/\partial t$ from Eqs. (13), (24), and (26).

7. Stoichiometry projection and single-reactional species flux

The single-reactional flux $J_k(\mathbf{x}, t)$ along the direction of reaction R_k can be decomposed into components of individual species using the predetermined stoichiometry $\mathbf{s}_k = (s_k^1, s_k^2)$. The x_1 and x_2 components of *stoichiometric projections* of $J_k(\mathbf{x}, t)$ are listed in Table II. The single-reactional species flux is formed as follows:

$$\mathbf{J}_k(\mathbf{x},t) \equiv (J_k^1(\mathbf{x},t), J_k^2(\mathbf{x},t)), \quad k = 1, \dots, 6,$$
 (27)

where $J_k^1(\mathbf{x},t)$ and $J_k^2(\mathbf{x},t)$ are listed in Table II. The single-reactional species velocity $\mathbf{v}_k(\mathbf{x},t) \in \mathbb{R}$ is $\mathbf{v}_k(\mathbf{x},t) \equiv \mathbf{J}_k(\mathbf{x},t)/p(\mathbf{x},t)$.

8. Total species flux and velocity

Following Eqs. (14) and (15), the total flux $\mathbf{J}_s(\mathbf{x}, t) \in \mathbb{R}^2$ is $\mathbf{J}_s(\mathbf{x}, t) = \sum_{k=1}^{m} \mathbf{J}_k(\mathbf{x}, t)$, where $\{\mathbf{J}_k\}$ is as specified in Eq. (27). The total species velocity $\mathbf{v}_s(\mathbf{x}, t) \in \mathbb{R}^2$ is $\mathbf{v}_s(\mathbf{x}, t) = \mathbf{J}_s(\mathbf{x}, t)/p(\mathbf{x}, t)$.

9. Overall behavior of Schnakenberg system

We examine the behavior of the Schnakenberg system with (a, b) = (10, 50) under two initial conditions, namely, that of the uniform distribution and $p(\mathbf{x} = (0, 0))|_{t=0} = 1$. We computed the time-evolving probability landscape $p = p(\mathbf{x}, t)$ using the ACME method. ^{12,43}

For the uniform distribution, the probability landscape in $-\log p(\mathbf{x}, t)$ at time t = 0.5 is shown in Fig. 4(a), where high probability regions are in blue. Its overall shape takes the form of closed valley, which is similar to an earlier study based on the Fokker-Planck model. 18 The trajectories of the flux field $\mathbf{J}_s(\mathbf{x}, t)$ at time t = 0.5 in the space of the copynumbers from different starting locations (marked by black arrows at the top and bottom) are shown in blue in Figs. 4 and 5. These trajectories depict the directions of the movement of the probability mass at different locations after traveling from the starting points. The heatmaps of the flux in $\log |J_s(\mathbf{x}, t)|$ and the velocity in $\log |v_s(\mathbf{x}, t)|$ are shown in Figs. 4(b) and 4(c), respectively. The flux lines are closed curves and are overall smooth. These closed flux lines reflect the oscillatory nature of the reaction system. The velocity has larger values at locations where the flux trajectories are straight lines [green and yellow regions in the upper right corner, Fig. 4(c)] but drops

TABLE II. Schnakenberg system reactional flux stoichiometry projections.

Reaction	$J_k^1(x_1, x_2, t) = s_k^1 J_k(x_1, x_2, t)$	$J_k^2(x_1, x_2, t) = s_k^2 J_k(x_1, x_2, t)$		
R_1	$r_1ap(x_1, x_2, t)$	0		
R_2	$-r_2(x_1+1)p(x_1+1,x_2,t)$	0		
R_3	0	$r_3bp(x_1,x_2,t)$		
R_4	0	$-r_4(x_2+1)p(x_1,x_2+1,t)$		
R_5	$r_5 \frac{x_1(x_1-1)x_2}{2} p(x_1, x_2, t)$	$-r_5\frac{x_1(x_1-1)x_2}{2}p(x_1,x_2,t)$		
R_6	$-r_6 \frac{(x_1-1)x_1(x_1+1)(x_1-2)}{6} p(x_1+1,x_2-1,t)$	$r_6 \frac{(x_1-1)x_1(x_1+1)(x_1-2)}{6} p(x_1+1,x_2-$		

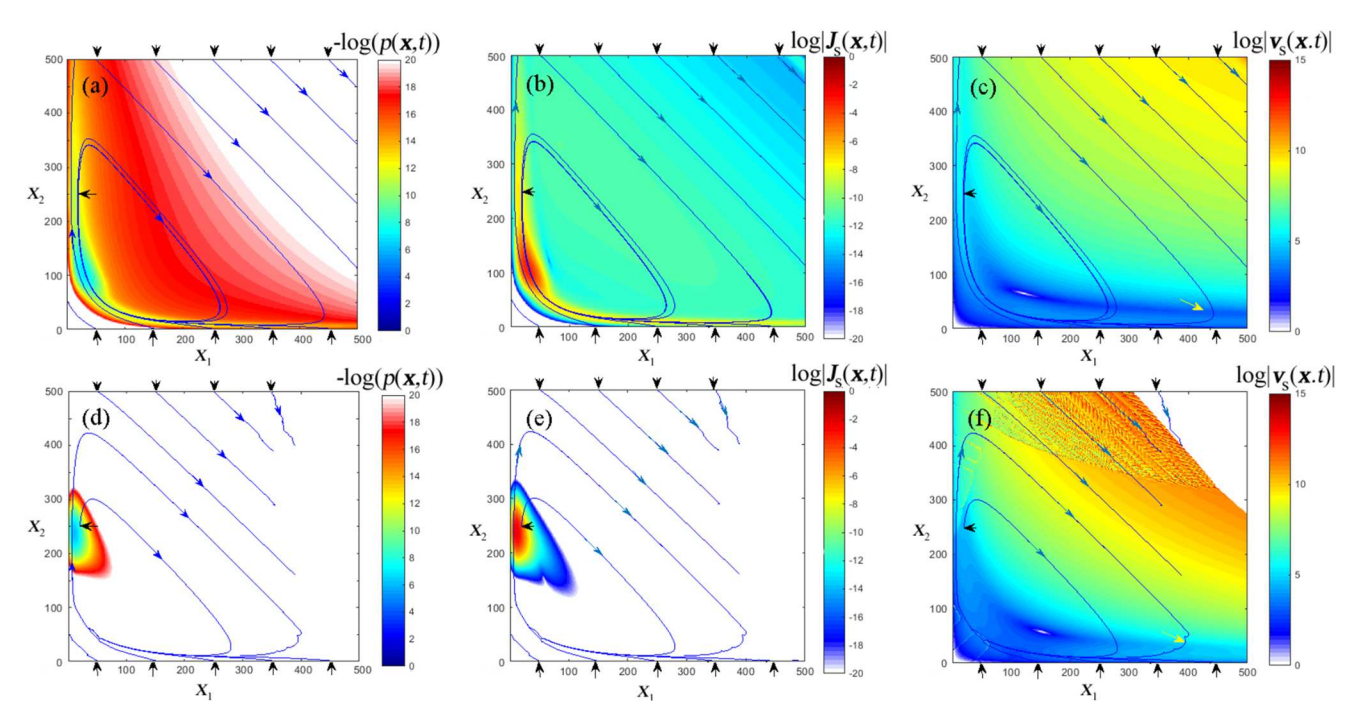


FIG. 4. The time-evolving probability landscape, flux, and velocity of probability mass in the Schnakenberg system with (a, b) = (10, 50) at t = 0.5, starting from the uniform distribution [(a)-(c)] and from the initial conditions of $p(\mathbf{x}=(0,0))|_{t=0}=1$ [(d)-(f)]. (a) and (d): the probability landscape in $-\log(p(\mathbf{x},t))$; (b) and (e): the corresponding value of flux in $\log |\mathbf{J}_s(\mathbf{x},t)|$; and (c) and (f): the \log absolute value of velocity $\log |\mathbf{v}_s(\mathbf{x},t)|$.

significantly when the trajectories make down-right turns (light and dark blue in the lower right corner, marked with an yellow arrow).

For the initial conditions of $p(\mathbf{x} = (0,0))|_{t=0} = 1$, $-\log p(\mathbf{x}, t)$ at time t = 0.5 is shown in Fig. 4(d), where high probability regions (blue) are located at a small neighborhood around $\mathbf{x} = (0, 250)$. The heatmaps of the flux in $\log |J_s(\mathbf{x}, t)|$ and the velocity in $\log |v_s(\mathbf{x}, t)|$ are shown in Figs. 4(e) and 4(f), respectively. The flux lines are closed curves and are overall smooth. The oscillating flux lines appear again [Figs. 4(d) and 4(f)], but not all form closed curves. Specifically, all flux lines which start at the upper region ($x_2 = 500$) become broken-off in the mid-region, where the probability mass becomes negligible, resulting in negligible flux as well, with its absolute value close to be zero. The maximum of the flux is reached at the peak of the probability landscape [Fig. 4(e)]. The heatmap of the probability velocity exhibits a similar pattern as that of uniform distribution [Fig. 4(f) vs. Fig. 4(c)]. The color palettes encoding the values of the velocity $\log |v_s(\mathbf{x}, t)|$ are not-smooth [Fig. 4(f)]. This is likely due to small numerical values of probability in this region.

We then examined the steady state behavior of the system at two conditions of the copy numbers of species A and B: (a, b) = (10, 50) and (a, b) = (20, 40). The probability landscape in $-\log(p(\mathbf{x}, t))$ for (a, b) = (10, 50) shown in Fig. 5(a) exhibits similar shape to that of Fig. 4. The probability values are higher in locations near the left $(x_1 = 0)$ and lower $(x_2 = 0)$ boundaries. The flux lines [Figs. 5(a)–5(c)] move from the upper left corner to the lower right corner and then make sharp right turns until reaching the neighborhood near the origin. Subsequently, they make right turns again and move upward, until the cycles

are closed. These closed flux curves move along the contours on the probability landscape. The absolute values of the flux [Fig. 5(b)] are largest near the boundaries of the probability surfaces ($x_1 = 0$ and $x_2 = 0$, red/orange colored ridge) and next along the flux lines on the diagonal. The flux has small values in the region above the diagonal (cyan and blue). The heatmap of the velocity [Fig. 5(c)] exhibits a different pattern, with its value dropping significantly in the small blue arch (see region pointed by the yellow arrow), where flux lines make turns in the lower region.

The probability landscape in $-\log(p(\mathbf{x}, t))$ for (a, b) = (20, 40) is shown in Fig. 5(d). While exhibiting overall similar pattern to that of (a, b) = (10, 50), the high probability regions are more concentrated in locations near the lower-left [Fig. 5(d)]. The flux lines [Figs. 5(d)–5(f)] are similar to those of (a, b) = (10, 50) corner but oscillate around much smaller contour, where $x_1 \le 200$ and $x_2 \le 300$. The close cycles of flux lines also move along the contours on the probability landscape.

The results obtained here are generally consistent with that obtained using the Fokker-Planck flux model computed from a landscape constructed using Gillespie simulations. 8,18 For example, the directions of the flux lines are the same. However, there are some differences. While the flux lines from the Fokker-Planck model exhibit oscillating behavior even in the boundary regions where $x_1 < 2$ or $x_2 < 2$, where reactions R_5 and R_6 cannot occur; hence, no oscillating flux is physically possible. No such inconsistency exists in our model. Furthermore, the system considered here is much larger, with hundreds of copies of X_1 and X_2 involved, whereas <10 copies of X_1 and X_2 were considered in Ref. 18.

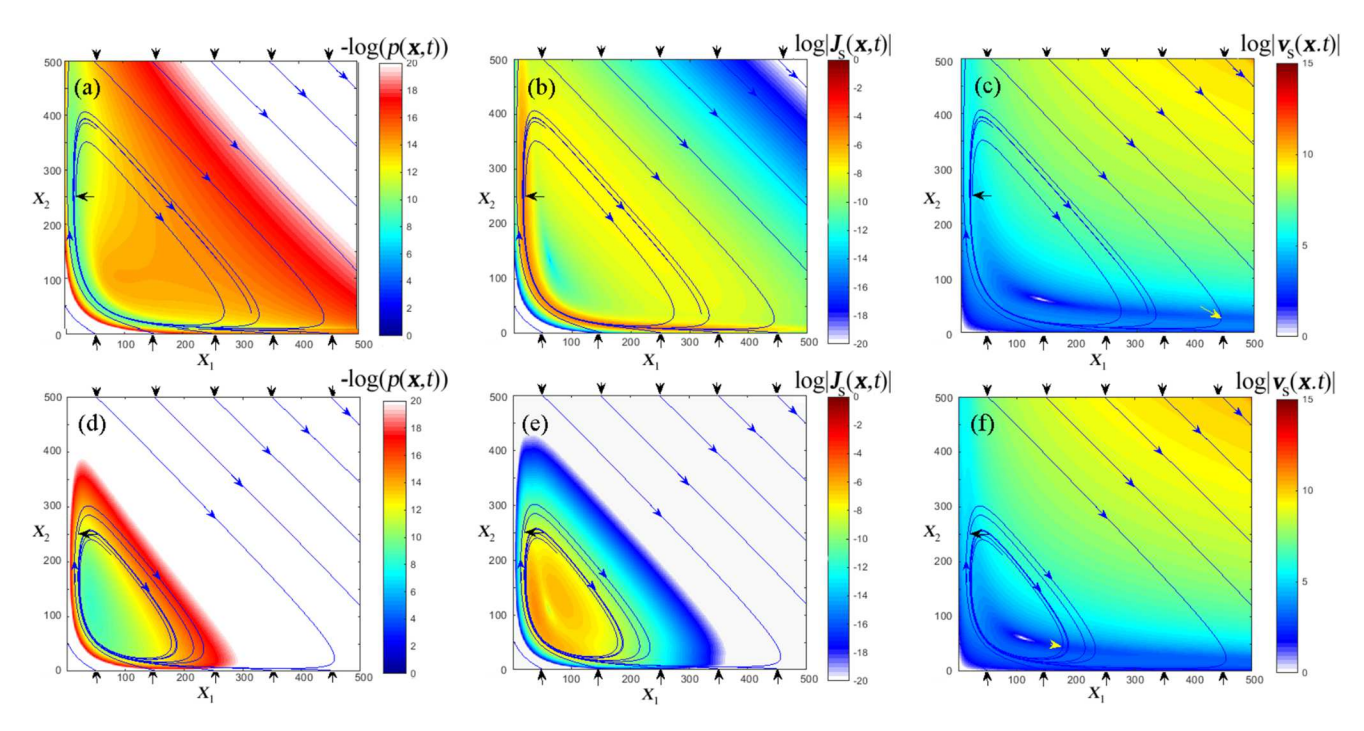


FIG. 5. The steady-state probability landscape, flux, and velocity of probability mass in the Schnakenberg system with (a, b) = (10, 50) [(a)–(c)] and (a, b) = (20, 40) [(d)–(f)]. (a) and (d): the probability landscape in $-\log(p(\mathbf{x}, t))$; (b) and (e): the corresponding values of flux in $\log |\mathbf{J}_s(\mathbf{x}, t)|$; and (c) and (f): the log absolute value of velocity $\log |\mathbf{v}_s(\mathbf{x}, t)|$.

IV. CONCLUSION

In this study, we introduce new formulations of discrete flux and discrete velocity for an arbitrary mesoscopic reaction system. Specifically, we redefine the derivative and divergence operators based on the discrete nature of chemical reactions. We then introduce the discrete form of continuity equation for the systems of reactions. We define two types of discrete flux, with their relationship specified. The reactional discrete flux satisfies the continuity equation and describes the behavior of the system evolving along directions of reactions. The species flux directly describes the dynamic behavior of the reactions such as the transfer of probability mass in the state space. Our discrete flux model enables the construction of the global time-evolving and steady-state flow-maps of fluxes in all directions at every microstate. Furthermore, it can be used to tag the fluxes of outflow and inflow of probability mass as reactions proceed. In addition, we can now impose boundary conditions, allowing exact quantification of vector fields of the discrete flux and discrete velocity anywhere in the discrete state space, without the difficulty of enforcing artificial reflecting conditions at the boundaries. 42 We note that the accurate construction of the discrete probability flux, velocity, and their global flow-maps requires the accurate calculation of the time-evolving probability landscape of the reaction network. This is made possible by using the recently developed ACME method. 12,43

As a demonstration, we computed the time-evolving probability flux and velocity fields for three model systems, namely, the birth-death process, the bistable Schlögl model, and the oscillating Schnakenberg system. We showed how flux and velocities converge to zero when the system reaches the steady-state in the birth-death process and the Schlögl

models. We also showed that the flux and velocity trajectories in the Schnakenberg system converge to the oscillating contours of the steady-state probability landscape, similar to an earlier study, ¹⁸ although there are important differences. Overall, the general framework of discrete flux and velocity and the methods introduced here can be applied to other networks and dynamical processes involving stochastic reactions. These applications can be useful in quantification of dynamic changes of probability mass, identification as well as characterization of the mechanism where movement of probability mass drives the system toward the steady-state. They may also aid in our understanding of the mechanisms that determined the non-equilibrium steady state of many reaction systems.

ACKNOWLEDGMENTS

Support from Grant Nos. NIH R35 GM127084 and NSF DMS-1714401 is gratefully acknowledged.

¹H. H. McAdams and A. Arkin, Trends Genet. **15**, 65 (1999).

²H. H. McAdams and A. Arkin, Proc. Natl. Acad. Sci. U. S. A. **94**, 814 (1997).

³M. Kærn, T. C. Elston, W. J. Blake, and J. J. Collins, Nat. Rev. Genet. 6, 451 (2005).

⁴V. Shahrezaei, J. F. Ollivier, and P. S. Swain, Mol. Syst. Biol. **4**, 196 (2008).

⁵M. B. Elowitz, A. J. Levine, E. D. Siggia, and P. S. Swain, Science 297, 1183 (2002).

⁶P. S. Swain, M. B. Elowitz, and E. D. Siggia, Proc. Natl. Acad. Sci. U. S. A. 99, 12795 (2002).

⁷M. Vellela and H. Qian, Bull. Math. Biol. **69**, 1727 (2007).

⁸D. T. Gillespie, J. Phys. Chem. **81**, 2340 (1977).

⁹H. D. Vo and R. B. Sidje, J. Chem. Phys. **147**, 044102 (2017).

¹⁰V. Wolf, R. Goel, M. Mateescu, and T. A. Henzinger, BMC Syst. Biol. 4, 42 (2010).

- ¹¹K. Burrage, M. Hegland, S. Macnamara, R. Sidje et al., in *Proceedings of* the A. A. Markov 150th Anniversary Meeting (Boson Books, Raleigh, NC, 2006), pp. 21-37.
- ¹²Y. Cao, A. Terebus, and J. Liang, Bull. Math. Biol. **78**, 617 (2016).
- ¹³Y. Cao and J. Liang, J. Chem. Phys. **139**, 025101 (2013).
- ¹⁴R. Zia and B. Schmittmann, J. Stat. Mech.: Theory Exp. 2007, P07012.
- ¹⁵C. Li, E. Wang, and J. Wang, Biophys. J. **101**, 1335 (2011).
- ¹⁶X.-J. Zhang, H. Qian, and M. Qian, Phys. Rep. **510**, 1 (2012).
- ¹⁷J. Wang, L. Xu, and E. Wang, Proc. Natl. Acad. Sci. U. S. A. 105, 12271 (2008).
- ¹⁸L. Xu, H. Shi, H. Feng, and J. Wang, J. Chem. Phys. **136**, 165102 (2012).
- ¹⁹R. Yuan, X. Wang, Y. Ma, B. Yuan, and P. Ao, Phys. Rev. E 87, 062109
- ²⁰M. Strasser, F. J. Theis, and C. Marr, Biophys. J. **102**, 19 (2012).
- ²¹J. T. Margaret, B. K. Chu, M. Roy, and E. L. Read, Biophys. J. **109**, 1746 (2015).
- ²²L. R. de Oliveira, A. Bazzani, E. Giampieri, and G. C. Castellani, J. Chem. Phys. 141, 065102 (2014).
- ²³C. Bianca and A. Lemarchand, Physica A **438**, 1 (2015).
- ²⁴C. Li and J. Wang, Proc. Natl. Acad. Sci. U. S. A. **111**, 14130 (2014).
- ²⁵J. Wang, L. Xu, E. Wang, and S. Huang, Biophys. J. **99**, 29 (2010).
- ²⁶C. Li and J. Wang, J. R. Soc., Interface **11**, 20140774 (2014).
- ²⁷Y. Tang, R. Yuan, G. Wang, X. Zhu, and P. Ao, Sci. Rep. 7, 15762
- ²⁸P. Sjöberg, P. Lötstedt, and J. Elf, Comput. Visualization Sci. 12, 37 (2009).
- ²⁹C. Y. Mou, J.-l. Luo, and G. Nicolis, J. Chem. Phys. **84**, 7011 (1986).
- ³⁰T. Schmiedl and U. Seifert, J. Chem. Phys. **126**, 044101 (2007).
- ³¹S. Xu, P. Sheng, and C. Liu, Commun. Math. Sci. **12**(4), 779 (2014).
- ³²D. Schultz, A. M. Walczak, J. N. Onuchic, and P. G. Wolynes, Proc. Natl. Acad. Sci. U. S. A. 105, 19165 (2008).
- ³³Y. Tang, R. Yuan, and P. Ao, Phys. Rev. E **89**, 062112 (2014).

- ³⁴N. G. Van Kampen, Stochastic Processes in Physics and Chemistry (Elsevier, 2007).
- ³⁵R. Grima, P. Thomas, and A. V. Straube, J. Chem. Phys. **135**, 084103 (2011).
- ³⁶A. Duncan, S. Liao, T. Vejchodský, R. Erban, and R. Grima, Phys. Rev. E 91, 042111 (2015).
- ³⁷D. T. Gillespie, J. Chem. Phys. **113**, 297 (2000).
- ³⁸F. Baras, M. M. Mansour, and J. Pearson, J. Chem. Phys. **105**, 8257 (1996).
- ³⁹P. Zhou and T. Li, J. Chem. Phys. **144**, 094109 (2016).
- $^{\rm 40}$ A. Bazzani, G. C. Castellani, E. Giampieri, D. Remondini, and L. N. Cooper, J. Chem. Phys. 136, 235102 (2012).
- ⁴¹J. M. Horowitz and M. Esposito, *Phys. Rev. X* **4**, 031015 (2014).
- ⁴²A. Ceccato and D. Frezzato, J. Chem. Phys. **148**, 064114 (2018).
- ⁴³Y. Cao, A. Terebus, and J. Liang, Multiscale Model. Simul. 14, 923 (2016).
- ⁴⁴B. J. Daigle, Jr., M. K. Roh, D. T. Gillespie, and L. R. Petzold, J. Chem. Phys. 134, 044110 (2011).
- ⁴⁵L. J. Allen, An Introduction to Stochastic Processes with Applications to Biology (CRC Press, 2010).
- ⁴⁶F. Schlögl, **Z**. Phys. **253**, 147 (1972).
- ⁴⁷H. Qian, S. Saffarian, and E. L. Elson, Proc. Natl. Acad. Sci. U. S. A. 99, 10376 (2002).
- ⁴⁸Y. Cao and J. Liang, J. Syst. Sci. Complexity 23, 896 (2010).
- ⁴⁹D. A. McQuarrie, J. Appl. Probab. **4**, 413 (1967).
- ⁵⁰Y. Cao and J. Liang, BMC Syst. Biol. **2**, 30 (2008).
- ⁵¹Y. Cao, H.-M. Lu, and J. Liang, Proc. Natl. Acad. Sci. U. S. A. 107, 18445
- ⁵²R. Shankar, *Principles of Quantum Mechanics* (Springer Science & Business Media, 2012).
- ⁵³H. Ge, M. Qian, and H. Qian, Phys. Rep. **510**, 87 (2012).
- ⁵⁴M. Vellela and H. Qian, J. R. Soc., Interface **6**, 925 (2009).
- ⁵⁵J. Schnakenberg, Rev. Mod. Phys. **48**, 571 (1976).